Distribution of alkali cations near Cu (111) surface in aqueous solution

Journal:	*Journal of Materials Chemistry A*
Manuscript ID	TA-COM-09-2020-008965.R1
Article Type:	Communication
Date Submitted by the Author:	04-Nov-2020
Complete List of Authors:	XI, CONG; Lawrence Berkeley National Laboratory, ; Tianjin University, Zheng, Fan; E O Lawrence Berkeley National Laboratory, Gao, Guoping; Lawrence Berkeley National Laboratory, Berkeley, Ye, Meng; Institute of Semiconductors, Chinese Academy of Sciences Dong, Cunku; Tianjin University, Du, Xiwen; Tianjin University, Institute of New-Energy Materials Wang, Lin-Wang; Lawrence Berkeley National Laboratory,

Distribution of alkali cations near Cu (111) surface in aqueous solution

Cong Xi,[ab] Fan Zheng,[b] Guoping Gao,[b] Meng Ye,[b] Cunku Dong,[a] Xi-Wen Du*[a] and Lin-Wang Wang*[bc]

It has been widely realized, in aqueous solution, metal cations near a catalytic surface in the Helmholtz layer can have significant influence on the catalytic reduction processes, from CO_2 reduction to H_2 generation. However, the exact nature of the cation distribution, the free energy profile, local coordination with water molecule, as well as the electrode potential dependence are still not known. For example, it is known water molecule can form some layer structures above the surface. Are the cations stay in some particular positions in the water layer? What is the free energy profile of a cation as a function of its position? What is the cation density at the surface for a given bulk concentration? How do their energy profiles depend on the electrode potential? What is the trend for different cations due to their size and chemistry difference? Answering these questions is essential to understand the role of cation in the aqueous based catalytic processes. In this work, using ab-initio molecular dynamics (AIMD) simulations with explicit water, we provide a systematic study of the above questions for the serial of alkali cations (Li^+, Na^+, K^+, Rb^+ and Cs^+) on both neutral and charged Cu (111) electrode (corresponding to electrode potential from -2.16 V to 1.56 V vs SHE). The results indicate that the alkali cations will stay near the electrode-electrolyte interface in a large potential range (from -2.16 V to 1.37 V). The free energy profile obtained from thermodynamics integration shows that Na^+ likes to stay near the interface, and it prefers in the odd layer of the water structure. A simple model is provided to explain the underlying reason for such behavior. We also find the surface concentration can be very high for a moderate bulk cation concentration, indicating the possible strong cation role in the catalytic process.

1. Introduction

Aqueous based catalysis is used to accelerate a wide range of electrochemical reactions, including reduction and oxidation processes to generate H_2/O_2 from water dissociation and convert CO_2 to carbon fuels to solve the energy and environmental crisis. It has now been realized that the explicit water molecule structure and the possibility of cation existence can play a major role in these reactions.[1-8] In aqueous based electrochemical reaction, salt is used often as electric conduction buffer layer to enhance the reaction. However, experimentally it has been demonstrated that cation species and their concentrations[6, 9-20] can also significantly affect the selectivity and activity of various electrocatalytic processes. For instance, the current density of CO_2 reduction reaction (CO_2RR) was found to increase significantly by increasing the sizes of the alkali metal cations[5-6, 10, 20-24] while Oxygen/Hydrogen involved reactions, like OER, ORR and HER, et al have a relatively sluggish

and non-monotonous response to the alkali metal sizes in electrolyte.[9, 25-28] Explanations of these phenomena have focused on specific interactions between cation and absorbate, the changes of the adsorption strength of the intermediates,[4, 6, 10, 25, 29] steric hindrance influence on active sites of adsorbates-$Mn^+(H_2O)_x$ cluster (M stands for cation species) [9, 30] and the change of reactants concentration resulted from cation hydrolysis.[24] It is notable that while the effect of alkali metal cation size on the activity of redox reactions has been known for over 50 years, a molecular level interpretation of mechanism of such impact has not been achieved.[13, 21] One challenge is that it is difficult to experimentally probe the microscopic atomic structure surrounding the reaction. As a result, a major part of the knowledge comes from theoretical simulations.

While many previous electrochemistry reactions were theoretical studied using continuum implicit solvent models,[31-35] it has been more and more widely realized that the explicit water molecule and its structure are important in order to understand the details of surface reactions.[3, 36-38] It is nevertheless challenging to investigate the explicit water effects due to their many degrees of freedom and associated thermodynamic fluctuations. To solve such problems, one approach is to use locally optimized monolayer water layer,[2, 4, 25, 39-41] although whether the structure conforms to the actual situation is not completely clear. Another approach is to employ thermodynamic bulk water ensembles at room temperatures from ab initio molecular dynamics,[3] which is more accurate but

a. Institute of New Energy Materials, School of Materials Science and Engineering, Tianjin University, Tianjin 30072, The People's Republic of China. E-mail: xwdu@tju.edu.cn

b. Materials Science Division, Lawrence Berkeley National Laboratory, Berkeley, California, 94720, USA. E-mail: lwwang@lbl.gov

c. Joint Center for Artificial Photosynthesis and Materials Science Division, Lawrence Berkeley National Laboratory, Berkeley, California, 94720, USA.

can be orders of magnitude more expensive in computation than using locally optimal structures. There are also challenges in using classical force fields to describe the surrounding water, for example, to study the cation and electrode potential effects.[42-44] Given these situations, and the need to include cation in these already complicated situations, an alternative approach is to first study the cation and water structure near the surface, then apply this knowledge in catalysis simulation, perhaps by using only a local water-cation cluster in accordance to the cation water structure obtained in prior calculations.

There are many previous theoretical studies regarding the pure water structure at the solid-liquid interface. Using AIMD simulations, Axel Groß and coworkers found hexagonal structure of water layers stable for at least 11 ps on clean and hydrogen-covered Pt (111) electrodes, and water pattern consisting of tetragons, hexagons, and octagons on Au (511) remained relatively stable after 10 ps at room temperature. However, these water patterns will be destroyed on other metal species or crystallographic planes.[45-46] There are also a lot of pioneering investigations for the structure and influence of water on electrocatalysis from Nørskov and Karen Chan et al,[47] by global optimization method. They found pentagonal and heptagonal water bonding network between stacked water layers as well as the persisting octagonal water sheet on IrO_2 (110) surface.[47] They also confirmed there was no fixed water pattern in the first water layer on Cu (211) surface.[48] In their serial investigations, to study the influence of water structure on the catalytic process, protonated/neutral water is not just accounted for stabilization role, but also sometimes directly involved in the reaction mechanism.[4, 40-41, 49-50] Despite all these studies, the role of the cations in interaction with water, especially at different electrode voltages, has not been fully addressed. Here, we provide a systematic theoretical study to investigate this problem. In particular, we study the alkali metal cations (Li^+, Na^+, K^+, Rb^+ and Cs^+), for a range of electrode potentials from -2.16 V to 1.56 V vs SHE. We use multiple layers of explicit water to ensure the accuracy of the simulation. We reported, for the first time, the stable positions of various cations and the local structures of the cation-water clusters on 3x3 Cu (111) surface. The Cu was chosen as the catalyst because it is widely used in CO_2 reduction reactions and exhibits excellent efficiency and selectivity for the products beyond CO, yet the role of cation in electrolyte has not been fully elucidated. Cu (111) single crystal surface was chosen since it is the most stable surface, and has been used in most theoretical studies under electrochemical conditions. All these are done with extensive AIMD simulations up to 50 ps duration with 136 atoms. We show that the cations can localize near the solid-liquid interface in a large range of electrode voltages, from -2.16 V to 1.37 V, which means the cation will exist even in oxidation as well as reduction conditions. Thermodynamics integration is used to the case of Na^+, yielding its free energy profile as a function of its position to the surface. We see local minimum and potential barrier, in corroboration with AIMD observed dynamic behavior. According to the free energy profile, we found surprisingly high surface density of Na^+ in moderate Na^+ bulk concentration. This indicates the abundance of cation at

the surface, thus the prominence of cation influence on the catalytic reaction. We believe all the information can be used to understand the catalytic process and to provide simplified structure model in future catalytic calculations.

2. Results and discussion

We first examined different positions of various cations on neutral Cu (111) by inserting the cations (Li^+, Na^+, K^+, Rb^+ and Cs^+) into the first water layer and equilibrating the system with ab-initio molecular dynamics for 50 ps. The effect of the initial positions on the final results was tested by putting the Sodium cation in 2.3 Å, 9.2 Å, and 16.3 Å from the substrate, and it was found that Na diffuses into the first water layer (~3 Å from the substrate) regardless of the initial positions within 4 ps (Fig. S1), which is a good indication that the final 3 Å configuration is stable and the initio position has no effect on the final intrinsic result. In Fig. 1, we see that all cations at first fluctuate tremendously up and down to accommodate interactions with the surrounding water and eventually stabilize around 3-4 Å above Cu after 30 ps, as indicated in the inset of Fig. 1. Nevertheless, there can be local minimum and free energy barriers. One example is K^+ as shown in Fig. 1. It was oscillating at position about 5.5 Å above Cu within the first 30 ps. We then artificially moved it to the first layer of the water around 3 Å, and it is kinetically stable over 20 ps afterwards, with no tendency to return back. The average distances of Li^+, Na^+, K^+, Rb^+ and Cs^+ to the first layer of Cu after the simulated equilibrium is reached are tabulated in Table. 1. All cations are stable at a distance of 3-4 Å from the Cu in the neutral system, which is consistent with previous results, where cations are believed to locate at 3-4 Å away from metal surfaces between the inner and outer Helmholtz planes.[1, 9, 24] To test the possible finite size effect of our 3x3 Cu (111) supercell, we have also used AIMD simulations to study the Cu-Na distance on a neutral 4x4 Cu (111) surface. Na^+ still stably stays at about 3 Å above the first layer of Cu surface (see Fig. S2 for more details), same as the 3x3 supercell result. This means the possible image-image interaction and correlation effect are rather small. We thus believe the 3x3 Cu (111) supercell is large enough for our purpose, and it will be used in the following investigations. In Ref. 4, it is reported that the local electric field caused by the cation charge can have influence within a radius of 5 Å, our 3-4 Å surface to cation distance indicates that the cation can indeed play an important role for catalytic reactions that take place on the surface.[4]

The order of cation distance to the first layer of Cu are Na^+ < Rb^+ < Cs^+ < K^+ < Li^+, which surprisingly does not follow monotonically with the cation size, unlike what is previously

Table 1. Average angle dipoles of different cation-water clusters and the mean cation-Cu distances in the process of AIMD simulations during 30-50 ps.

Cation species	Li	Na	K	Rb	Cs
Angle dipole	-0.38	-0.11	-0.22	-0.17	-0.18
Cation-Cu distance	3.88	3.02	3.54	3.29	3.41

ARTICLE
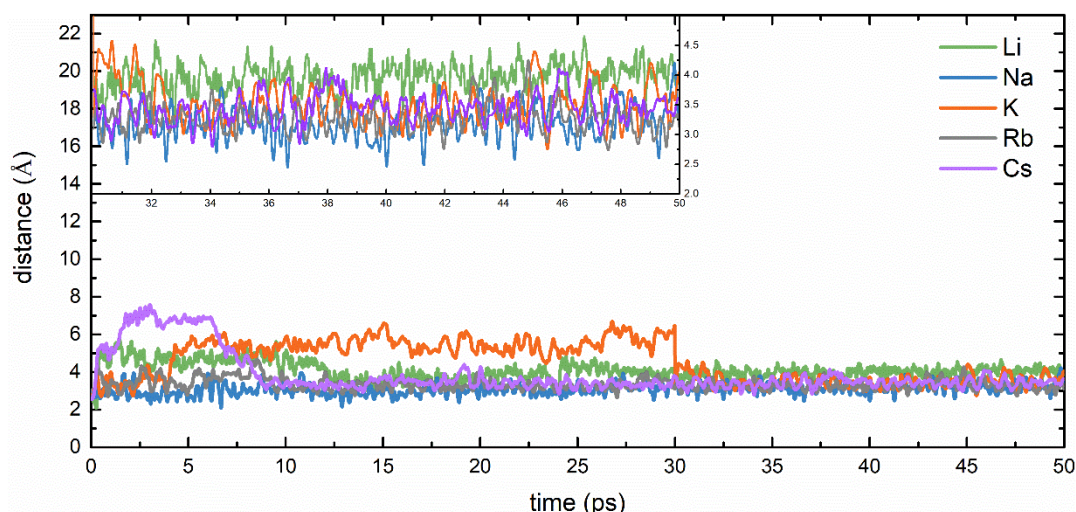
Fig. 1 The change of distances between cations and the first layer of Cu for 50 ps in ab -initio MD calculation. All cations tend to stably stay 3-4 Å away from the Cu. The inset figure of cation-Cu distance in 30-50 ps is shown to clarify specific fluctuation range of cations and the order of their distances to metal surface. For the K$^+$ case, at 30ps, we have artificially replaced it to the first layer of the water.

assumed as used in the modified Poisson-Boltzmann (PB) continuum solvent model.[7] The reason for this non-monotonic relationship lies in the local structure in the cation-water clusters and their interactions with the Cu surface. To shed more light on such cation-water cluster, we calculated the average radial distribution functions of the cation and the surrounding water molecule (the O atom in the water molecule) within the radius of 12 Å for the simulations of Fig. 1 at the equilibrium condition. The results are shown in Fig. 2a. There are clear peaks in the cation-O radial distribution function within 2.5 Å, 3.0 Å, 3.6 Å, 3.8 Å and 4.0 Å cut off for Li$^+$, Na$^+$, K$^+$, Rb$^+$ and Cs$^+$, respectively, indicating the first cation-water shell. The integrated quantity of this first peak is around 3.9 to 6.6. The average number of water molecules around K$^+$ is about 6.6, followed by Cs$^+$ and Rb$^+$, with about 6.2 and 5.8 water molecules, respectively. There are about 4.4 water molecules

for Na$^+$, which agrees with the previous ionization potential analysis that reflects the stable hydration of sodium contains 4 water molecules.[51] Li$^+$ has the smallest number, 3.9, of water molecules surrounding it, perhaps due to steric effect. The number of surrounding water molecule is a result of competition between the Coulomb interaction (and perhaps some state hybridization interaction) between the O and cation atoms and the steric effect for water molecules. Unfortunately, the number of water molecule around each cation does not correspond to its distance to Cu (111) surface in a monotonic fashion. Li has the smallest number of waters, its distance to the surface is the largest, while K has the largest number of waters, but its distance is not closest to the surface. To shed more light on this, we put forward a concept of an angle dipole for the cation-water first shell cluster, which is defined as the average cosine value of the angle θ between the cation-O line to the
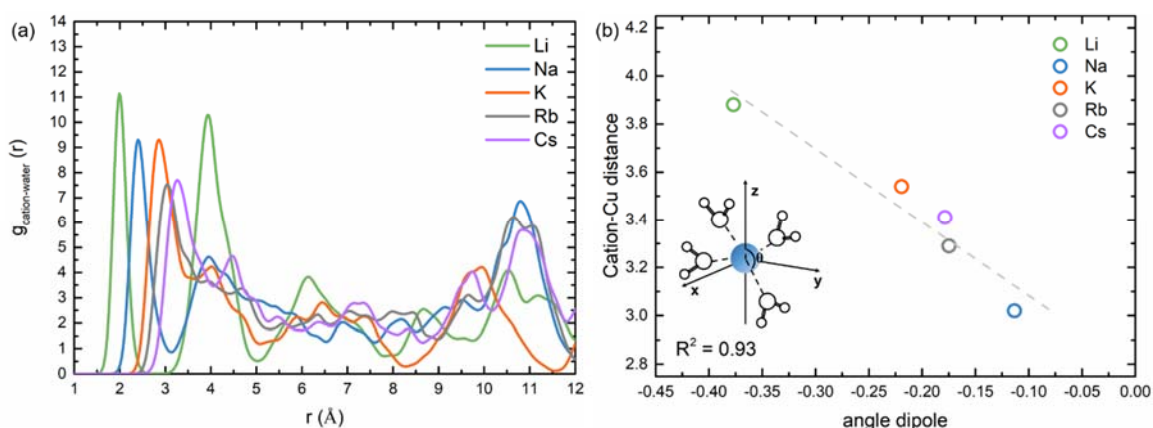
Fig. 2 (a) Comparison of the mean radical distribution functions of cation-O (in H2O) obtained in ab initio simulations after the structure is in equilibrium. (b) Correlation of cation-substrate distance with cation-O angle dipole moment defined as cos(θ). Only the water molecule with its O position lower than the cation (e.g., θ > 90 degree) is accounted in the calculation. The inset structure is an illustration of angle θ with the central blue ball being the cation.

ARTICLE

vertical z-axis (as indicated in the inset illustration of Fig. 2b). Only the water molecule with θ > 90 degree is accepted in the average. Thus, it probes the completeness of the lower hemisphere towards the surface. The more negative value of the angle dipole indicates more water molecules exist between the cation and the surface. Note for an intact uniform half sphere, as in the case of a complete water shell when the cation is far away from the surface, the angle dipole of the cation is -0.45. This for example is true for our later Na cation simulation when it is far away from the surface. In the case where the cation is close to the surface, as shown in Fig. 2b, we see that Li has an angle dipole close to -0.45. This means it has a complete lower half sphere (hence perhaps the whole water shell). Thus, this angle dipole can be used as a measure for whether the water shell is intact, or is dissociated (at least for the lower hemisphere). It turns out this angle dipole correlates with the cation-surface distance well, with a linear correlation number being R^2=0.93 as shown in Fig. 2b. This means the best indicator for the cation surface distance is the cation-water shell completeness, instead of the number of water molecules surrounding each cation, or the cation radius. The stronger and more intact of the shell is, the larger cation to surface distance will be. The Li^+ probably has a strongest cation-water binding, thus its water shell is intact, ending up with the largest cation-surface distance despite of having the smallest radius. For weaker water shell, due to the tendency of the cation to be attracted to the surface (e.g., due to the imagine charge attraction as will be discussed later), the water shell can be broken. However, in general, this water shell strength is a result of combination of the cation size and steric effect, so it is not a simple function of the cation size.

The above calculations are done at neutral charge, where the electrode potential is at its flat band potential (for Cu (111), it corresponds to -0.3 V relative to SHE[52-53]). In the electrochemical reduction reactions, such as CO_2, O_2, N_2 reduction reactions (i.e. CRR, ORR, NRR), the electrode is in more negative voltage relative to SHE, and the electrode is in an electron enriched charge state. The surface electric field is pointing towards the solid surface. Thus, the positive cation will be more tightly bounded to the surface. To test this, we have used Na^+ as our example. We performed some short ab initio molecular dynamics simulations, with electrode voltage ranges from neutral to -1.23, and -2.16 V relative to SHE. Fig. S3 shows that, for all these cases, the Na^+ are located near the surface, and the average distances are more or less the same. What is more interesting is to look at what happens at positive electrode voltage, where the electrode is in electron depleted state, thus might repulse the positive cation. To evaluate the effects of oxidative positive electrode potential on the position

of cation, we carried out a series of long AIMD simulations with different positive electrode potentials.

It is worth to discuss the technical details for how to carry out AIMD with different electrode potentials. Ideally, one can carry out a grand canonical simulation with fixed electrode potential and fluctuating total number of electron. But such simulations are quite expensive. As pointed out in our recent work,[54] the effects of different electrode potentials can be captured by fixed charge calculations with the adequate charges. Thus, in above simulations, different electrode potentials are achieved by changing the total number of electrons in the system. A depleted number of electrons is used to yield a positive electrode potential. The electrode potential for a given extra charge is evaluated by comparing the electrode Fermi energy and the middle "water" layer potential using an implicit solvent model simulation and calibrating with the SHE potential based on the result of zero charge calculation. The use of implicit solvent model instead of explicit water model for this purpose is to reduce the fluctuation in the evaluation of the average water potential in the simulation. By design, the dielectric response in the implicit solvent model should adequately describe the explicit water response, thus can provide the adequate potential in the water region. More detailed discussions for the calibration and the relationship between the charge and potential are described in the supplemental information and illustrated in Fig. S4. In actual explicit water simulation, there is also an issue of electrode potential (represented by its Fermi energy) fluctuation. In a fixed charge calculation, the Fermi energy can fluctuate with an average root mean square of 200 meV (Fig.S4). However, after averaging over a typical simulation length of a few ps, the uncertainty of the potential reduces to about 16 meV (see the SI for more details). One should consider the stochastic nature of this as in a NVT simulation for the temperature, where the fluctuation also exists.

Another subtle issue is the uniform charge background treatment in a charged system periodic boundary condition simulation. In a periodic boundary condition plane wave code, a uniform background charge is used to make the system neutral when solving the Coulomb potential. This means a uniform charge exists in the water region. Although, artificial, this can be considered as representing the effect of possible counter ions in the solvent. Another possible treatment is to use Poisson-Boltzmann solution in which the counter ion effect is included following the Boltzmann distribution. To test the possible effects of these different treatments, we have solved the potential profiles using implicit solvent model, with Poisson-Boltzmann equation, and without Poisson-Boltzmann equation (hence the same compensating background charge treatment

as in our explicit water simulation). They yield almost the same potential profile for the same extra charge case as shown in Fig.S5. This means this background charge issue does not have a significant impact. Furthermore, we have also carried out an AIMD simulation with a Cu/explicit water/implicit water model, with the implicit water region represented by an implicit solvent model with Poisson-Boltzmann equation. The Na^+ results at two different electrode potentials are almost the same as in our above simulation without implicit water layer (Fig.S5). We will thus use 3x3 Cu/explicit-water model simulations throughout the rest of our study.

Fig. 3 shows the MD trajectories represented by the distance of Na^+ to the surface as functions of time. Again, 50 ps simulations are done for 6 positive oxidation potentials. When the positive potential is less than 1.37 V, Na^+ is still stable near the double layer, and with the cation-surface distance more or less unchanged. When the voltage increases to 1.37 V, Na^+ starts to escape upward at about 30 ps to 5 Å above the first layer of Cu. We see a large fluctuation of the Na-surface distance. When the voltage increases to 1.56 V, the cation completely escapes away from the metal surface and reaches the middle of the simulated water slab, which is 10 Å away from the metal surface. This is surprising, since it means the electrode surface will still be covered with Na^+ for oxidation reactions under 1.37 V. We do note that, in OER voltage conditions, other species, especially anions, might cover the surface as well, and it can also influence the cation absorption. For example, experimental literature reported that the presence of OH* absorbate can shorten the distance between cations and metal surfaces through a non-covalent interaction.[55] Besides, the metal electrode can be oxidized to metal oxide in the oxidative condition, further enhancing the interaction between the cation and surface oxides. Thus, the actual situation can be more complicated. But overall, we conclude that, despite the electrode potential repulsing, and an out pointing electric field,

the cation can still stay near the surface even in some oxidization conditions with positive electrode voltage.

We next like to study the cation position relative to water structure near the solid-liquid interface. There are many previous studies for pure water structure without cation. Some experimental work has discovered perfect hexagonal hydrogen bond network of monolayer water structure on Pt (111) using x-ray absorption and x-ray emission[56] as well as periodicity water pattern along the (001) direction on TiO_2 (110) through scanning tunneling microscopy.[57] Here, comparing to the in-plane structure of each layer, we are more interested in z direction water layer, where water forms layer structures when there are multiple water layers. AIMD of $Cu-H_2O$ system without cation is carried out. A Gaussian-broadened average of water density (using its O atom as its center), and its H-O-H dipole orientation are calculated and shown in Fig. 4. The layered structure of the water can be clearly inferred from Fig. 4a. There are seven layers of water in our simulated system, and the first peak is positioned at 3 Å away from the metal surface, coinciding with the Na^+ cation position. The H-O-H orientation dipole for each water molecule is defined as:

$$\frac{(H_{1,z}-O_z)+(H_{2,z}-O_z)}{2} \tag{1}$$

where the subscript z indicates the vertical z coordinate, the subscripts 1 and 2 indicate the two H atoms within a water molecule. Thus, a positive dipole means the molecule has a H-O-H angle with O pointing towards the surface. The results in Fig. 4a indicate that with pure water on Cu (111), the dipole direction is rather weak, without strong orientation preference. In our multilayer water structure, we also didn't find stable water pattern at the first layer, although our 3x3 supercell lateral cross section is commensurate with the hexagonal water structure. We found ever-changing quadrilateral, pentagon, hexagonal and heptagonal water patterns, but none of them is stable over time. This qualitatively agrees with reported results
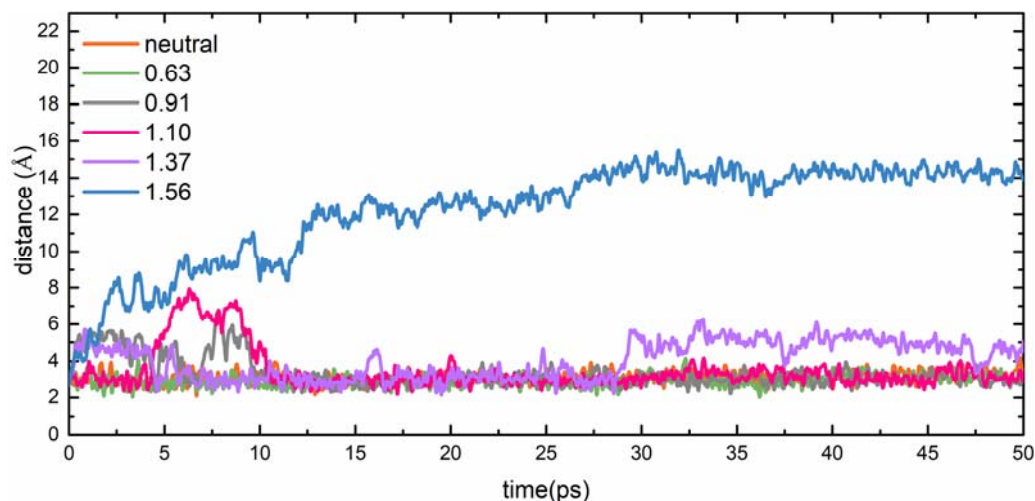
Fig. 3 The change of distances with time between Na and the first layer of positively charged Cu for 50 ps in ab-initio MD calculation. Na would stably locate near the solid-liquid interface until 1.37 V voltage is exerted on Cu electrode and would escape away from the interface when 1.56 V voltage is provided.

ARTICLE
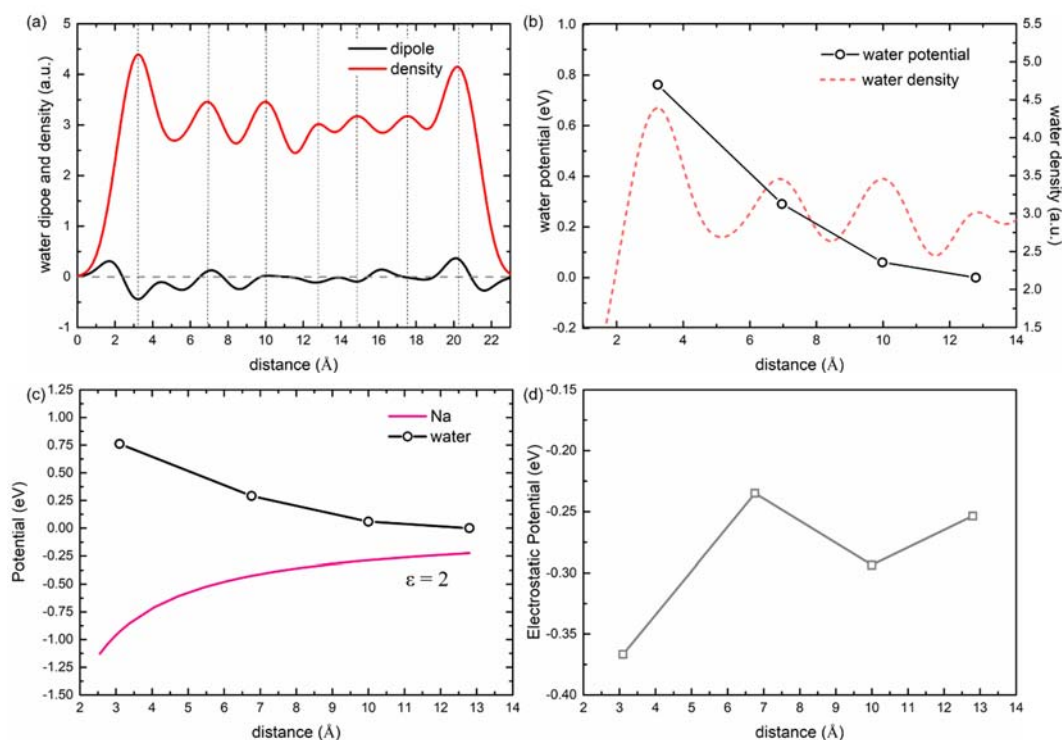
Fig. 4 (a) pure water density and orientation (b) water layer potential for the first four water layers when there is no cation in electrolyte. (c) Pure water potential (black) and electromagnetic potential of Na (red) verse distance to solid-liquid interface. (d) the possible reason for position preference of the cation based on the sum potential of water and Na.

that claim the first layer of water can have 4, 5 or 7 water rings on Cu, Ag or Au, deviating from the purely hexagonal water structure on Pt (111).[46, 48, 58-60] This is probably because the stable water structure depends on strong binding of the water molecule to the substrate atoms like Pt (111), which is lacking with Cu (111) surface.

The pure water simulation can also give us the potential profile in the Helmholtz layer close to the surface. The time-averaged 1s-core levels of oxygen at different z-positions are calculated during AIMD. The results are reported in Table S1 and shown in Fig. 4b. This result (which is calculated at the neutral charge) shows a positive potential near the surface (or say an electric field pointing away from the surface). The difference from the surface layer and the middle of the water region can be 0.8 V. If this is the only potential Na^+ is subjected to, the Na^+ should move towards the center of the system. There could also be interaction between the Na^+ and the peaks of the water layer densities shown in Fig. 4a, but nevertheless since there are water layers peaks both near the surface and in the middle of the water slab, that cannot be used to explain the Na^+ position to be close to the Cu surface. Note, the Helmholtz layer potential is often used together with Boltzmann distribution to

estimate the cation concentration. In such a simple picture, a positive potential will push away all the cations, in contrast to our direct simulated results (under zero charge of the total system). This is also against the experimental observation, e.g., by synchrotron radiation method, which found K^+, Cs^+, or even Ba^{2+} are located at 3.5-4.1 Å above various metal surfaces. [9, 55, 61]

We thus cannot use the electrostatic potential obtained from the O atom core level to estimate the free energy profile of the cation. To yield a more accurate free energy profile, we have used free energy perturbation (FEP) method, i.e., thermal dynamics integration to obtain the free energy difference at different cation positions. [62-63] To do that, we first performed AIMD starting from 24 distinct cation distances from the Cu surface. For each of these simulations, the Na^+ is allowed to move laterally, but not vertically, so it will preserve its distance to the surface. Each system was equilibrated with a thermostat set at 300 K under Nose-Hoover algorithm for 1000 fs. After equilibration, the simulation was continued for another 5000 fs, during which the z direction force on the Na^+ is averaged. Such averaged force as a function of the Na^+ position is shown in Fig. 5a. We also estimated the error bar of the average force based

on our average time duration and the force-force fluctuation decay time as discussed in the SI. There is some force fluctuation when Na$^+$ is far away from the surface. However, when the Na$^+$ is close to the surface, the results are quite reliable. It is not clear why there is a dip in the force near 7.5 Å, but the result looks repeatable. We do acknowledge that the relatively small 3x3 cross section might provide some artificial constraints and correlations in the lateral direction, thus can cause some complicated oscillating behaviors, but we believe the overall force, especially the free energy after the force integration, should be more reliable. The integration of the average force along the z direction will give us the free energy profiles, [62-63] which is shown in Fig. 5b. As we can see, the curve in Fig. 5b is much smoother than that in Fig. 5a, and the small fluctuations in the force have been integrated out. The positions of zero force in Fig. 5a correspond to local potential extreme points in Fig. 5b, with a local maximum potential at 5.5 Å, a local

minimum point at 8.4 Å and a global energy minimum point at 2.9 Å above the interface. This global free energy minimum at 2.9 Å coincides with the average position of Na during the long MD simulation as shown in Fig. 1. The existence of the local minimum besides the global minimum agrees with the phenomena we found in the AIMD for the case of K shown in Fig. 1, where the trajectory can be stuck in a local minimum z position.

To understand the free energy profile, and its possible correlation to the water structure, we have analysed water density and dipole when Na is placed at the free energy extreme points (i.e. 2.9 Å, 5.5 Å, 8.4 Å, 11.4 Å above Cu surface). The results are shown in Fig. 5c-f. First, by comparing the water density and dipole moment with the pure water case shown in Fig. 4a, we found that there is significant influence of the Na atom on the water layer density and the polarization. It is clear, where ever there is Na$^+$, there will be a water density peak, this
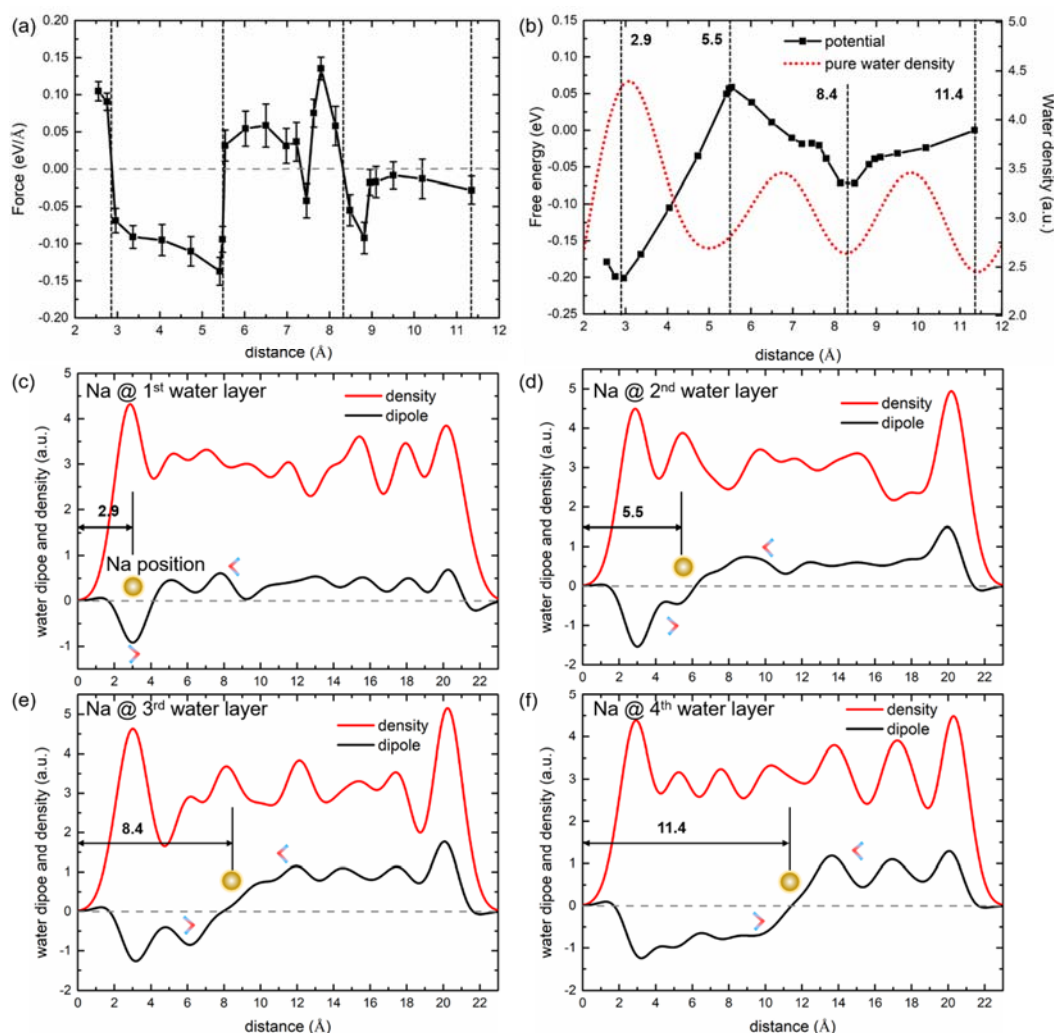
Fig. 5 (a) the mean force on Na in z-axis at different heights from metal surface. The error bars are quantified by the standard error of the mean and correlation time analysis in each dynamic trajectory. (b) free energy of Na from infinity to metal surface through the integration of the mean force. Comparison of water density and dipole when Na is fixed in the (c) first, (d) second, (e) third and (f) fourth water layer. The yellow ball representing Na is to help follow the cation position and the arrow stands for water to help identify water orientation, with red end representing Oxygen and two blue ends representing Hydrogen atoms.

ARTICLE

is despite the fact the Na$^+$ itself will occupy a certain amount of space at that z position. This water density peak is probably due to the Na-water shell structure. From the water polarization, we can see the O atom is pointing towards the Na$^+$, as expected. It is also noticeable that the global free energy minimum corresponds to the first water layer peak in the pure water case. Although this is not true for other cations, like Li, this nevertheless might mean in the case of Na$^+$ at least, the match between the Na-water shell, and the pure water first layer peak might have lowered its energy, and helped to locate its free energy global minimum there.

It is nevertheless interesting why the free energy profile is not a monotonic curve as in the electrostatic potential shown in Fig. 4b. To understand this, we realized another possible effect, which is the image potential from the Cu substrate. For a given point charge q at distance d above a metal surface, there will be an image charge $-q$ at $-d$ position, hence introduce a $-q^2/2d$ attractive potential. Due to the dielectric screening effect of the water, this attractive position should be $-q^2/2\varepsilon d$. Here, at such nanoscale distance, one cannot use the water bulk dielectric constant. The ε is likely to be much smaller than the bulk water dielectric constant. If we take $\varepsilon=2$, we yield an attractive potential shown in Fig. 4c. The sum of this attractive potential and the original electrostatic potential without Na$^+$ shown in Fig. 4d does produce a curve with a global minimum and a barrier, with qualitative agreement with the final free energy curve shown in Fig. 5b. Although this is not a rigorous derivation, and it ignores the possible complicated cation-water local interaction, it does provide a qualitative picture to understand
the free energy profile, and possibly provide a simple model for such profile.
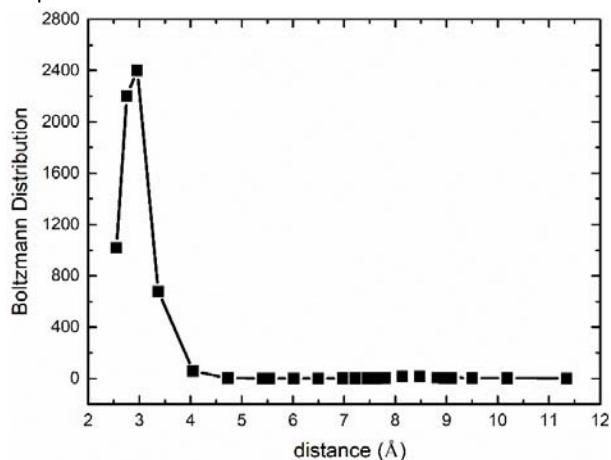
Fig. 6 the probability distribution of Na versus its distances from metal surface.

Lastly, we like to use the free energy profile shown in Fig. 5b to calculate the concentration of the Na$^+$ at different distances from the surface. One way is to use Boltzmann distribution to calculate the local concentration as: [64]

$$p(d)=p_{bulk}\,exp(-\frac{G(d)-G_{bulk}}{kT})$$

(2)

where p(d) is the cation 3D concentration at distance d from the surface, and G(d) is the Gibbs free energy shown in Fig. 5b at distance d. We can approximate d=11.4 Å is the bulk value, and p$_{bulk}$ is the cation bulk concentration. For a given cation concentration (e.g., 0.1 mol/L), we can reach an extremely high concentration around 2.5-3.5 Å, about 230 mol/L. This is due to the large ΔG of 0.2 eV. This means this surface will be saturated with cation. However, based on the free energy profile, the cation will form a layer at about 3.0 Å. Thus, it is more appropriate to estimate the 2D layer cation density. It is not clear what thickness one should use to convert the 3D density to 2D density. One can integral p(d) over the valley, but it is not clear whether Eq. (2) will still be valid given the narrow valley. An alternative way to estimate the cation surface concentration at the valley of the potential profile in Fig. 5b is to view the valley as a 2D layer system, and it is in equilibrium with the rest of the 3D solvent system. In another word, the whole electrolyte is divided into one two-dimensional system, with a cation surface density of σ = N$_s$ /A (A is the area), and a three-dimensional system, with a cation volume density of n = N$_v$ /V (V is the volume). To reach an equilibrium, the cation chemical potential in surface and volume must be the same:

$$\mu_{surface}= \mu_{bulk}$$

(3)

The surface and bulk chemical potential of cation are respectively provided by

$$\mu_{surface}= \Delta G + \mu_{2D}+ \mu_{vib}$$

(4)

$$\mu_{bulk}= \mu_{3D}$$

(5)

where ΔG, μ$_{2D}$ and μ$_{3D}$ represent the cation free energy difference as shown in Fig. 5b, the chemical potential of a free 2d system with concentration σ, and the chemical potential of a free 3D system with concentration n. Besides, μ$_{vib}$ is the 1-dimensional (z-direction) phonon vibrational free energy using the potential valley profile of Fig. 5b as a harmonic oscillator. We can use ideal gas model to calculate μ$_{2D}$ and μ$_{3D}$ in the equation (6) and (7) shown below (see derivation details in supporting):

$$\mu_{2D}= - kT\,ln\left(\frac{mkT}{2\pi\hbar^2\cdot\sigma}\right)$$

(6)

$$\mu_{3D}= - kT\,ln\left[\frac{1}{n}\left(\frac{mkT}{2\pi\hbar^2}\right)^{3/2}\right]$$

(7)

where m is the cation mass. μ$_{vib}$ in Eq. (4) could be obtained according to harmonic oscillator model in the following equation:

$$\mu_{vib}= \hbar\omega\left(\frac{1}{2}+ \frac{1}{e^{\hbar\omega/kT}-1}\right) -kT\left[\frac{\hbar\omega/kT}{e^{\hbar\omega/kT}-1}- ln\left(1- e^{-\hbar\omega/kT}\right)\right]$$

(8)

ARTICLE

where ω is the phonon mode that can be estimated from the energy curve. Combining above formulas, we get an equation for the surface density σ as:

$$\sigma = n \left(\frac{2\pi\hbar^2}{mkT}\right)^{1/2} e^{\frac{-\Delta G - \mu_{vib}}{kT}} \quad (9)$$

In our calculation, we found ω is 7.24×1012 S^{-1}, and $\mu_{vib} = -0.0044$ eV. For the most common cases in experiment, 0.1 mol/L Na^+, we estimate σ to be 1.6 $Na^+/Å^2$ at 3 Å above Cu surface. This is obviously too high, larger than the possible packing density of Na cation. This is because in the above estimation, we have used ideal gas approximation for the 3D and 2D case. In a solvent, the volume should be replaced by a movable volume for the cation in the liquid, which should be much smaller, and that should reduce the possible concentration. Another factor which has not been taken into account is the cation-cation repulsing due to their Coulomb interaction and possible water shell interaction when the concentration is high. Nevertheless, the above estimation indicates the cation can reach saturation surface density, perhaps saturated to the close pack density when their water shell is considered. This means the surface is covered with cation, and the cation can indeed have significant influence on the catalysis.

3. Conclusions

The alkali cation distribution at the Cu (111) surface is studied using AIMD. The information of such cation distribution is necessary for better understanding of their roles in surface catalysis, and to provide structure model for future theoretical investigation of catalytic process. Extensive systematic AIMD calculations are carried out, and thermal dynamic integrations are used to calculate the free energy profile. Water structure analysis and its interaction with the cation are used to understand the free energy profile. Through our simulation, we have the following main conclusions:

(1) The cation surface distance does not simply follow the cation size through the alkali metal serial. Instead, the distance is correlated with the cation-O dipole moment, or say the degree of water shell dissociation. This means for cation with strong water shell, its distance to the surface is farthest. For Li^+, it has a strong cation-water interaction, and its water shell is mostly intact, which results in the largest distance. On the other hand, for Na^+, half of the water shell is broken, resulting in the shortest distance. As a result, there is no water between Na^+ and the Cu surface;

(2) In a wide range of electrode voltages (-2.16 to 1.37 V relative to SHE electrode level), the Na^+ will stay near the surface around 3 Å. This means, even in some oxidation conditions (1.37 V), the cation can play an important role in the surface catalysis;

(3) Although the electrostatic potential in the Helmholtz layer is monotonic (as shown in Fig. 4b), the Na^+ Gibbs free energy profile is not monotonic. It has a global minimum near 3 Å, but a barrier at around 5.5 Å. This barrier behavior agrees with the dynamic behavior observed in the AIMD;

(4) The non-monotonic behavior is probably a result of the electrostatic potential, and the charge image interaction with the surface. The cation and water layer interaction might also play a role. For Na^+, which has the shortest cation-surface distance, its position coincides with the first water layer density peak of pure water on top of Cu;

(5) There is a strong cation water correlation, represented by a cation-water shell. This is demonstrated by the influence of the average water density peak by the existence of the cation, and the water dipole direction pointing to the cation;

(6) Using the Gibbs free energy profile, the thermodynamically estimated Na^+ surface concentration is extremely high, indicating the possible saturation of the cation density near the surface. This also shows the abundant availability of cation near the surface, which can significantly influence the surface catalytic process.

Conflicts of interest

There are no conflicts of interest to declare.

Acknowledgements

References

1   A. Bagger, L. Arnarson, M. H. Hansen, E. Spohr and J. Rossmeisl, *J. Am. Chem. Soc.,* 2019, **141**, 1506-1514.
2   H. Shin, H. Xiao and W. A. Goddard III, *J. Am. Chem. Soc.,* 2018, **140**, 6745-6748.
3   T. Cheng, H. Xiao and W. A. Goddard III, *J. Am. Chem. Soc.,* 2016, **138**, 13802-13805.
4   L. D. Chen, M. Urushihara, K. Chan and J. K.Nørskov, *ACS Catal*., 2016, **6**, 7133-7139.
5   A. Murata and Y. Hori, *Bull. Chem. Soc. Jpn.,* 1991, **64**, 123-127.
6   E. Pérez-Gallent, G. Marcandalli, M. C. Figueiredo, F. Calle-Vallejo and M. T. Koper, *J. Am. Chem. Soc.,* 2017, **139**, 16412-16419.
7   S. Ringe, E. L. Clark, J. Resasco, A. Walton, B. Seger, A. T. Bell and K. Chan, *Energy Environ. Sci.,* 2019, **12**, 3001-3014.
8   H. H. Kristoffersen, T. Vegge and H. A. Hansen, *Chem Sci.,* 2018, **9**, 6912-6921.
9   D. Strmcnik, D. F. Van Der Vliet, K. C. Chang, V. Komanicky, K. Kodama, H. You, V. R. Stamenkovic and N. M. Markovic, *J. Phys. Chem. Lett.,* 2011, **2**, 2733-2736.
10 J. Resasco, L.D. Chen, E. Clark, C. Tsai, C. Hahn, T.F. Jaramillo, K. Chan and A.T. Bell, *J. Am. Chem. Soc.,* 2017, **139**, 11277-11287.

11 D. A. Rakov, F. Chen, S. A. Ferdousi, H. Li, T. Pathirana, A. N. Simonov, P. C. Howlett, R. Atkin and M. Forsyth, *Nat. Mater.,* 2020, 1-6.

12 S. Kaneco, K. Iiba, H. Katsumata, T. Suzuki and K. Ohta, *J Solid State Electrchem.,* 2007, **11**, 490-495.

13 A. N. Frumkin, *Trans. Faraday. Soc.,* 1959, **55**, 156-167.

14 C. Stoffelsma, P. Rodriguez, G. Garcia, N. GarciaAraez, D. Strmcnik, N. M. Markovic and M.T. Koper, *J. Am. Chem. Soc.,* 2010, **132**, 16127-16133.

15 E. Sitta, B. C. Batista and H. Varela, *Chem. Commun.,* 2011, **47**, 3775-3777.

16 G. García, C. Stoffelsma, P. Rodriguez and M. T. Koper, *Surf. Sci.,* 2015, **631**, 267-271.

17 C. McDonnell-Worth and D. R. MacFarlane, *RSC Adv.,* 2014, **4**, 30551-30557.

18 B. A. Previdello, E. G. Machado and H. Varela, *RSC Adv.* 2014, **4**, 15271-15275.

19 G. A. Ragoisha, T. A. Auchynnikava, E. A. Streltsov and S.M. Rabchynski, *Electrochim. Acta,* 2014, **122**, 218-223.

20 M. R. Thorson, K. I. Siil and P.J. Kenis, *J. Electrochem. Soc.*, 2012, **160**, F69.

21 W. Paik, T. N. Andersen and H. Eyring, *Electrochim. Acta,* 1969, **14**, 1217-1232.

22 G. Z. Kyriacou and A. K. Anagnostopoulos, *J. Appl. Electrochem.*, 1993, **23**, 483-486.

23 Y. Hori and S. Suzuki, *Bull. Chem. Soc. Jpn.,* 1982, **55**, 660-665.

24 M. R. Singh, Y. Kwon, Y. Lum, J. W. Ager III and A. T. Bell, *J. Am. Chem. Soc.,* 2016, **138**, 13006-13012.

25 C. Ding, X. Zhou, J. Shi, P. Yan, Z. Wang, G. Liu and C. Li, *J. Phys. Chem. B.,* 2015, **119**, 3560-3566.

26 J. D. Michael, E. L. Demeter, S. M. Illes, Q. Fan, J. R. Boes and J. R. Kitchin, *J. Phys. Chem. C.,* 2015, **119**, 11475-11481.

27 J. Tymoczko, V. Colic, A. Ganassin, W.Schuhmann and A. S. Bandarenka, *Catal. Today,* 2015, **244**, 96-102.

28 J. Zaffran, M. B. Stevens, C. D. Trang, M. Nagli, M. Shehadeh, S. W. Boettcher and M. Caspary Toroker, *Chem. Mater.,* 2017, **29**, 4761-4767.

29 S. A. Akhade, I. T. McCrum and M. J. Janik, *J. Electrochem. Soc.,* 2016, **163**, F477.

30 D. Strmcnik, K. Kodama, D. van der Vliet, J. Greeley, V. R. Stamenkovic and N. M. Marković, *Nat. Chem.,* 2009, **1**, 466-472.

31 I. Borukhov, D. Andelman and H. Orland, *Electrochim. Acta,* 2000, **46**, 221-229.

32 O. Andreussi, I. Dabo, N. Marzari, *J. Chem. Phys.,* 2012, **136**, 064102.

33 K. Mathew, R. Sundararaman, K. Letchworth-Weaver, T. A. Arias and R. G. Hennig, *J. Chem. Phys.,* 2014, **140**, 084106.

34 K. Mathew, V. C. Kolluru, S. Mula, S. N. Steinmann and R. G. Hennig, *J. Chem. Phys.,* 2019, **151**, 234101.

35 J. Tomasi, B. Mennucci and Cammi, R. *Chem. Rev.,* 2005, **105**, 2999-3094.

36 T. Cheng, H. Xiao and W. A. Goddard III, *J. Phys. Chem. Lett.,* 2015, **6**, 4767-4773.

37 J. H. Montoya, C. Shi, K. Chan and J. K. Nørskov, *J. Phys. Chem. Lett.,* 2015, **6**, 2032-2037.

38 J. A. Gauthier, S. Ringe, C. F. Dickens, A. J. Garza, A. T. Bell, M. Head-Gordon, J. K. Nørskov and K. Chan, *ACS Catal*., 2018, **9**, 920-931.

39 J.A. Gauthier, M. Fields, M. Bajdich, L.D. Chen, R.B. Sandberg, K. Chan and J.K. Nørskov, *J. Phys. Chem. C.,* 2019. **123**, 29278-29283.

40 X. Liu, P. Schlexer, J. Xiao, Y. Ji, L. Wang, R. B. Sandberg, M. Tang, K. S. Brown, H. Peng, S. Ringe and C. Hahn, *Nat. Commun*., 2019, **10**, 32.

41 X. Liu, J. Xiao, H. Peng, X. Hong, K. Chan and J. K. Nørskov, *Nat. Commun.,* 2017, **8**, 15438.

42 J. I. Siepmann and M. Sprik, *J. Chem. Phys*., 1995, **102**, 511-524.

43 D. T. Limmer, A. P. Willard, P. Madden and D. Chandler, *PNAS* 2013, **110**, 4200-4205.

44 D. T. Limmer, A. P. Willard, P. A. Madden and D. Chandler, *J. Phys. Chem. C.,* 2015, **119**, 24016-24024.

45 T. Roman and A. Groß, *Catal. Today,* 2013, **202**, 183-190.

46 A. Gross, F. Gossenberger, X. Lin, M. Naderian, S. Sakong and T. Roman, *J. Electrochem. Soc.,* 2014, **161**, 3015-3020.

47 J. A. Gauthier, C. F. Dickens, L. D. Chen, A. D. Doyle and J. K. Nørskov, *J. Phys. Chem. C.,* 2017, **121**, 11455-11463.

48 T. Ludwig, J. A. Gauthier, K. S. Brown, S. Ringe, J. K. Nørskov, K. Chan, *J. Phys. Chem. C.,* 2019, **123**, 5999-6009.

49 V. Tripković, E. Skúlason, S. Siahrostami, J. K. Nørskov and J. Rossmeisl, *Electrochim. Acta,* 2010, **55**, 7975-7981.

50 K. Jiang, R. B. Sandberg, A. J. Akey, X. Liu, D. C. Bell, J. K. Nørskov, K. Chan and H. Wang, *Nat. Catal.,* 2018, **1**, 111-119.

51 R. N. Barnett and U. Landman, *Phys. Rev. Lett.*, 1993, **70**, 1775.

52 J. J. McMullen and N. Hackerman, *J. Electrochem. Soc.,* 1959, **106**, 341.

53 G. J. Clark, T. N. Andersen, R. S. Valentine and H. Eyring, *J. Electrochem. Soc.*, 1974, **121**, 618.

54 G. Gao, and L.W. Wang, J.Catal., 2020, 391, 530.

55 C. A. Lucas, P. Thompson, Y. Gründer and N. M. Markovic, *Electrochem. commun.,* 2011, **13**, 1205-1208.

56 H. Ogasawara, B. Brena, D. Nordlund, M. Nyberg, A. Pelmenschikov, L. G. M. Pettersson and A. Nilsson, *Phys. Rev. Lett.,* 2002, **89**, 276102.

57 G. Serrano, B. Bonanni, M. Di Giovannantonio, T. Kosmala, M. Schmid, U. Diebold, A. Di Carlo, J. Cheng, J. VandeVondele, K. Wandelt and C. Goletti, *Adv. Mater. Interfaces,* 2015, **2**, 1500246.

58 H. Ibach, *Surf. Sci.,* 2010, **604**, 377-385.

59 X. Lin and A. Groß, *Surf. Sci.* 2012, **606**, 886-891.

60 A. Michaelides and K. Morgenstern, *Nat. Mater.,* 2007, **6**, 597-601.

61 Y. Liu, T. Kawaguchi, M. S. Pierce, V. Komanicky and H. You, *J. Phys. Chem. Lett.,* 2018, **9**, 1265-1271.

62 J. G. Kirkwood, *J. Chem. Phys.,* 1935, **3**, 300-313.

63 D. Frenkel and B. Smit, Understanding molecular simulation: from algorithms to applications, Elsevier, 2001, Vol. 1.

64 D. McQuarrie, Statistical mechanics university science books, Sausalito, 2000, pp 222-223.